THE ASTROPHYSICAL JOURNAL, 332:328–334, 1988 September 1

SMALL GRAINS AND *IRAS* COLORS

F. BOULANGER,[1,2] C. BEICHMAN,[1] F. X. DÉSERT,[2,3] G. HELOU,[1] M. PÉRAULT,[2] AND C. RYTER[4]

Received 1988 January 4; accepted 1988 February 19

ABSTRACT

We study how infrared colors of dust emission from the interstellar medium vary with the energy density of the radiation field on the basis of *IRAS* observations of the California Nebula. The data suggest that color variations result from a combination of equilibrium emission from large grains, and nonequilibrium emission from small grains, with destruction of the small grains emitting at 12 μm at high energy density; we estimate that 80% of these small particles are destroyed for an energy density in ultraviolet photons larger than 50 times that of the average interstellar radiation field in the solar neighborhood. In a color-color diagram, $I_\nu(60\ \mu m)/I_\nu(100\ \mu m)$ versus $I_\nu(12\ \mu m)/I_\nu(25\ \mu m)$, the California Nebula measurements at various distances to the ionizing star ξ Per follow a sequence similar to that of galaxies. This result shows that the position of a galaxy along this sequence is a measure of the intensity of the radiation field in the regions responsible for the infrared emission.

Subject headings: infrared: sources — interstellar: grains — nebulae: individual (NGC 1499) — nebulae: reflection

I. INTRODUCTION

Early observations in the mid- and far-infrared of the star-forming region M17 led Andriesse (1978) to suggest the existence in the interstellar medium of grains with sizes of 10 Å exhibiting temperature fluctuations up to about 150 K. Later, the detection of extended near-infrared emission in a few reflection nebulae (Sellgren, Werner, and Dinerstein 1983) provided evidence for the existence of even smaller grains with temperatures fluctuating up to 1000 K. The AFGL observations (Price 1981) had also revealed intense mid-infrared emission (10–20 μm) from the Galactic plane, proving the existence of a population of grains with temperatures of a few 100 K throughout the Galaxy (Pajot *et al.* 1986), but it was not clear whether these hot grains were small particles in the interstellar medium or big grains in circumstellar dust shells (Cox, Krugel, and Mezger 1986). By detecting 12 and 25 μm emission from the different components of the nearby interstellar medium—H II regions, atomic and molecular clouds (see Boulanger and Pérault 1988 and references therein)—*IRAS* has since established small grains as a pervasive component of interstellar dust.

Spectra of the reflection nebulae NGC 2023 and NGC 7023 (Sellgren *et al.* 1985) show that a large fraction of the emission of small grains between 2 and 13 μm is associated with the infrared features at 3.3, 3.4, 6.2, 7.7, 8.6, and 11.3 μm; on the basis of this result, polycyclic aromatic molecules (PAHs), identified as the carriers of the infrared features (Léger and Puget 1984), have been considered as good candidates to explain the emission from the interstellar medium in the near-infrared and the 12 μm band of *IRAS* (Puget, Léger, and Boulanger 1985). Since little is known about the emission of PAHs at wavelengths longer than 15 μm, it is unclear whether the 25 μm emission comes from aggregates of PAHs or other small particles.

For energy densities comparable to the local interstellar radiation field (ISRF) the $I_\nu(60\ \mu m)/I_\nu(100\ \mu m)$ color is not significantly dependent on the intensity of the heating of dust (Ryter, Puget, and Pérault 1987; Boulanger and Pérault 1988); this result, together with the fact that the ratio between the 60 and 100 μm emission is higher than one expects from graphite, amorphous carbon, and silicate grains (hereafter "large grains") in thermal equilibrium with the local ISRF (Draine and Lee 1984), suggests that grains which are not in thermal equilibrium (hereafter "small grains") are necessary to explain not only the 12 and 25 μm emission but also part of the 60 μm emission from the interstellar medium (Draine and Anderson 1985).

For very small particles the time between photon absorptions is larger than the cooling time, and the spectral distribution of the emission is independent of the intensity of the radiation field. On the other hand, the emission from large grains gradually shifts to shorter wavelengths as the equilibrium temperature increases. The combination of the non-equilibrium emission from small grains with the equilibrium emission from large grains determines the dependence of *IRAS* colors on the energy density of the radiation field. This dependence can be empirically investigated by studying the distribution of infrared emission around stars exciting reflection nebulae or H II regions (Castelaz, Sellgren, and Werner 1987; Ryter, Puget, and Pérault 1987); in this paper we study the variation of infrared colors with the energy density of the radiation field on the basis of *IRAS* observations of the California Nebula (§ II). A simple analytical model of the infrared emission from a mixture of small and large grains is presented in § III. In § IV, comparing data and model, we suggest that a large fraction of the small grains emitting at 12 μm are destroyed at high energy densities; the California Nebula data are also used to discuss colors of galaxies. The results of this study are summarized in § V.

[1] Infrared and Processing Analysis Center, California Institute of Technology.
[2] Ecole Normale Supérieure, Paris.
[3] Laboratory of Astronomy and Solar Physics, Goddard Space Flight Center.
[4] Service d'Astrophysique, Centre d'Etudes Nucléaires de Saclay, Gif-sur-Yvette, France.

II. THE CALIFORNIA NEBULA

We investigate the dependence of infrared colors on the energy density of the radiation field by studying the distribution of the infrared emission around the star ξ Per. This star is the source of ionization of the California Nebula (NGC 1499); it has an apparent visual magnitude corrected for extinction of 3.0 mag and is classified as an O7.5 III star (Hoffleit and Jaschek 1982; Bohlin, Savage, and Drake 1978; Walborn 1972). For the temperature scale of Morton (1979) the effective temperature of ξ Per is 34,000 K, and the bolometric correction is -3.3 mag (Snow and Jenkins 1977); from the visual magnitude and the bolometric correction, we derive the integrated flux of the star, $F = \int f_\nu \, d\nu = 3.3 \times 10^{-8}$ W m^{-2}. There are some uncertainties on effective temperatures of O stars; Garmany, Conti, and Chiosi (1982) give an effective temperature of 37,500 K for ξ Per, which implies a bolometric correction 25% higher; in the following we assume that $F = 3.3 \pm 0.8 \times 10^{-8}$ W m^{-2}.

To study the variation of infrared colors with distance to the star, we co-added the *IRAS* survey observations on a $8° \times 8°$ grid with 1′ pixels. The zodiacal light and the emission associated with the foreground and background interstellar medium were subtracted by fitting a wedge over several positions around the nebula. A color-coded image of the 12, 60, and 100 μm emission is presented in Figure 1 (Plate 4). The distribution of matter in the nebula has been discussed by Bohnenstengel and Wendker (1976) on the basis of radio continuum observations; close to the star the density of matter is low, $n_e \approx 1$ cm^{-3}; proceeding northeast of ξ Per, on the brightest filaments of NGC 1499, the density goes up to about 50 cm^{-3}; the northwest side of the nebula is bordered by a dust cloud observed in CO by Elmegreen and Elmegreen (1978) and Ungerechts and Thaddeus (1987). The filaments visible on optical photographs of the nebula suggest that the matter is stratified in several ionization fronts approximately parallel to the line of sight; such a geometry is particularly favorable to our study because layers of matter at different distances do not overlap along the line of sight.

Figure 2 shows the distribution of the infrared emission along a cut going through ξ Per and the peak of the radio continuum map of Bohnenstengel and Wendker (1976); the position angle of the cut is 56°.3. Zodiacal light, and Galactic emission unrelated to the nebula, were subtracted by fitting a linear baseline over emission minima at both ends of the cut; we estimate the uncertainties on the 12, 25, 60, and 100 μm fluxes in Figure 2 to be of the order of 0.15, 0.2, 0.75, and 2.5 MJy sr^{-1}, respectively. The emission profiles were combined to produce the color profiles of Figure 3. For a distance θ from the star the energy density in ultraviolet radiation at the tangent point is given by the formula:

$$u = F/(c\theta^2) + 0.15 \text{ eV cm}^{-3}$$
$$= 325(\theta/5')^{-2} + 0.15 \text{ eV cm}^{-3} ,$$

where the additional term of 0.15 eV cm^{-3} represents the contribution of the ultraviolet part of the average interstellar radiation field (ISRF; Mathis, Mezger, and Panagia 1983); excitation from the star to the different positions in the nebula is small enough to be neglected; u is about 2000 times the ISRF value, $u_{\rm ISRF}$, at 5′ from the star, and about 6 times $u_{\rm ISRF}$ at a distance of 100′.

The color profiles in Figure 3 show how the different infrared colors vary with the intensity of the radiation field. Colors measured at 100′ from ξ Per are comparable to the average colors for $u = u_{\rm ISRF}$ obtained by Boulanger and Pérault (1988) for Galactic latitude profiles at $|b| > 10°$. With increasing energy density, the $I_\nu(12\ \mu\text{m})/I_\nu(25\ \mu\text{m})$ ratio follows a plateau and then drops steadily; the $I_\nu(25\ \mu\text{m})/I_\nu(60\ \mu\text{m})$ ratio decreases at low energy density, reaches a minimum at about 30′ from the star, and increases close to the star. In the simple picture where dust grains are all in thermal equilibrium, one expects these two colors, like the $I_\nu(60\ \mu\text{m})/I_\nu(100\ \mu\text{m})$ ratio, to be an increasing function of energy density. We show in the next section that the peculiar behavior of the $I_\nu(12\ \mu\text{m})/I_\nu(25\ \mu\text{m})$ and $I_\nu(25\ \mu\text{m})/I_\nu(60\ \mu\text{m})$ colors can be simply explained if part of the emission comes from small particles radiating with a spectrum roughly independent of the energy density. In Figure 3 the $I_\nu(60\ \mu\text{m})/I_\nu(100\ \mu\text{m})$ color goes from 0.2 to 1, while the energy density u varies by a factor of about 300; equilibrium emission from grains having an emissivity varying as a power law of the frequency with an index between 0 and 2 gives for the same increase in energy density a color variation twice as large. Ryter, Puget, and Pérault (1987) found around two stars in Ophiuchus an increase in the $I_\nu(60\ \mu\text{m})/I_\nu(100\ \mu\text{m})$ ratio much closer to what is expected from emission of large grains. Colors in the California Nebula are probably affected by the integration of the emission along the line of sight, since it is likely that along each line of sight a significant fraction of the emission comes from grains at energy densities lower than the one at the tangent point; in their work Ryter *et al.* circumvented this problem by measuring colors of narrow filaments, which enabled them to use very local baselines.

In their study Ryter, Puget, and Pérault (1987) also found that the ratio of mid-infrared to far-infrared emission, parametrized by the quantity $R(12,\ 60 + 100) = \nu I_\nu(12\ \mu\text{m})/[\nu I_\nu(60\ \mu\text{m}) + \nu I_\nu(100\ \mu\text{m})]$, decreases as the energy density goes from a few tenths to a few hundreds of eV cm^{-3}; for this range of energy densities the 12 μm emission comes from small grains, and most of the far-infrared emission from large grains; therefore, the observed decrease implies that the small particles emitting at 12 μm are destroyed in regions of intense heating. Similarly, in the California Nebula we find that $R(12, 60 + 100)$ decreases by about a factor of 10 from energy densities of 1 ($\theta \approx 100'$) to 20 ($\theta \approx 30'$) eV cm^{-3}; no further decrease is seen for higher energy density (Fig. 3). Besides the overall decrease, the $R(12, 60 + 100)$ profile presents several localized enhancements. The peak at a distance of 67′ from the star, also apparent on the $I_\nu(12\ \mu\text{m})/I_\nu(25\ \mu\text{m})$ profile, coincides with the crossing of one of the main filaments seen on the optical photograph, and the infrared image (Fig. 1) of NGC 1499; the second main filament crossed at a distance of 45′ from the star does not appear as clearly. The two other peaks at 84′ and 95′ coincide with bumps in the 12 μm profile which are slightly visible at 25 μm but are not seen at 60 and 100 μm; these peaks do not have any obvious optical counterpart.

III. ANALYTICAL MODEL

To discuss the results obtained in the previous section, we use an analytical model of the infrared emission from a mixture of small and big grains. The emissivity of the large grains is assumed to follow a power law with an index n; the temperature of these grains is given by the equilibrium relation

$$E_a = AT_{\rm eq}^{n+4} , \quad (1)$$

where E_a is the rate of absorption of energy per grain and A is a

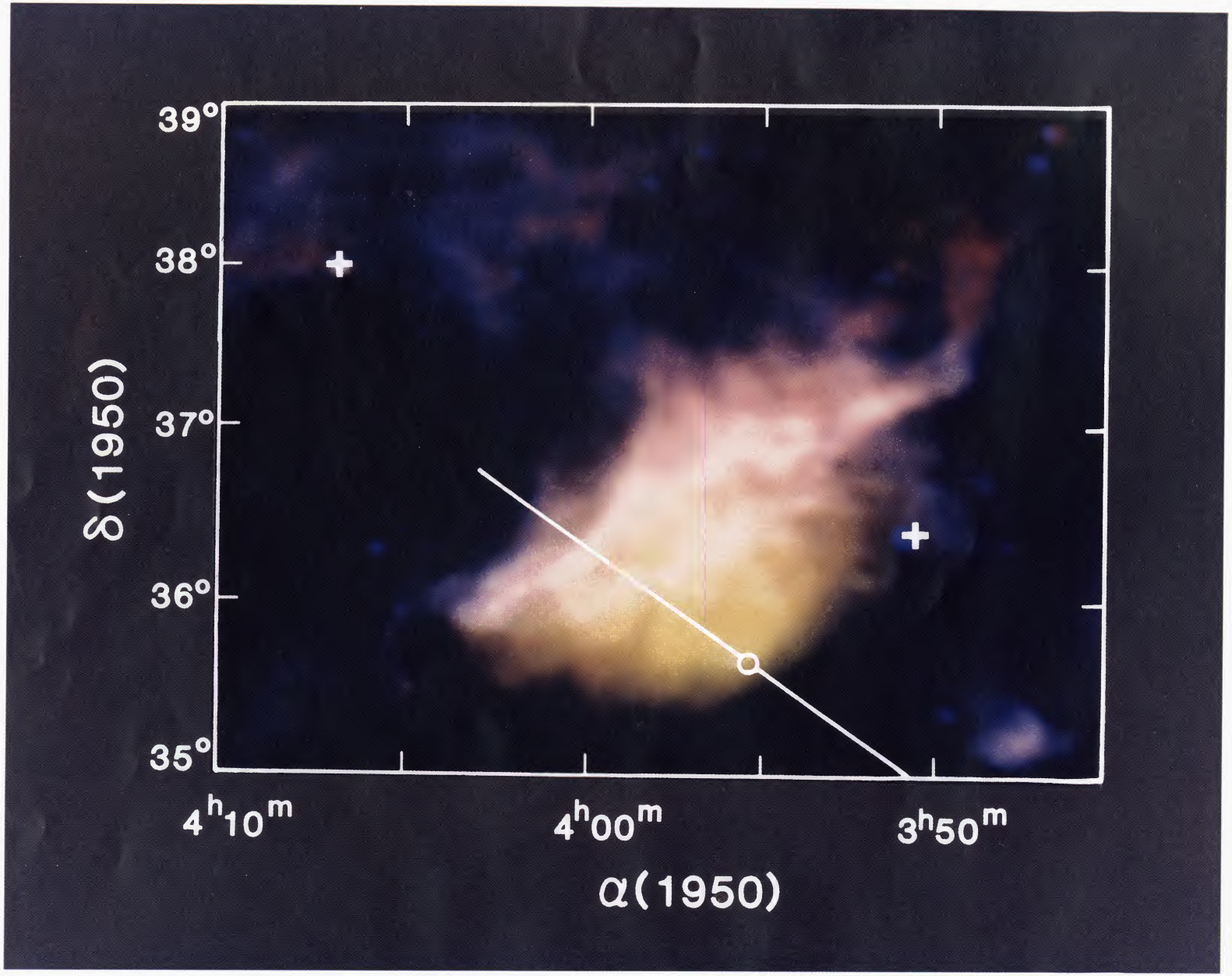

FIG. 1.—Color-coded image of the infrared emission from the California Nebula. The intensity of the blue color is based on the 12 μm emission, the green on the 60 μm, and the red on the 100 μm. A circle marks the position of the star ξ Per; the segment indicates the position of the cut used to study color variations. Emission and color profiles along this cut are presented in Figs. 2 and 3. Crosses indicate reference sources used to reconstruct absolute positions.

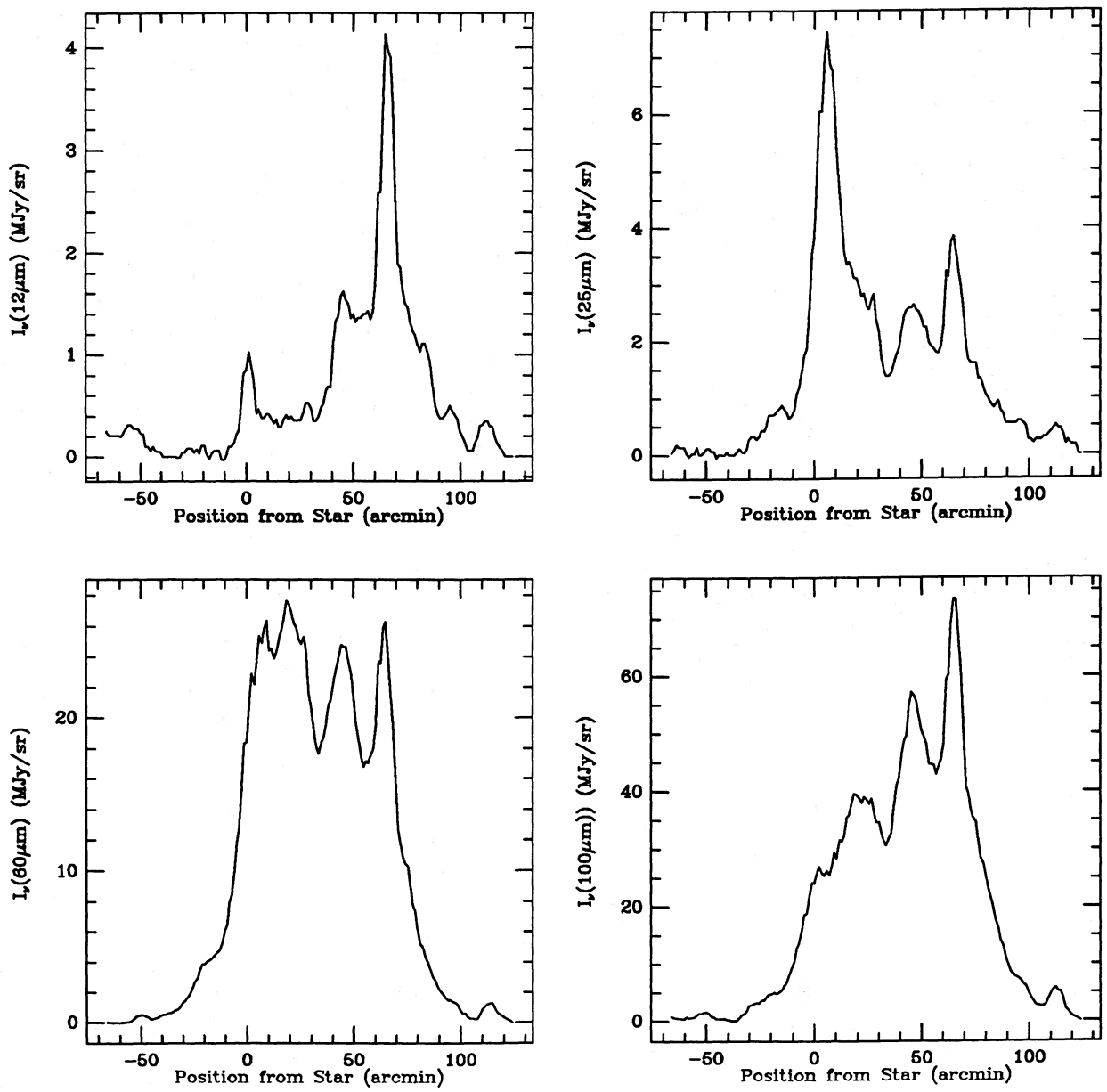

FIG. 2.—Profiles of the 12, 25, 60, and 100 μm emission along the cut drawn in Fig. 1

normalization constant depending on the emissivity of the grains. To simplify the problem, we keep the spectral distribution of the incident radiation field constant; E_a then scales linearly with the energy density u, and by normalizing u to 1 for $T_{eq} = 20$ K, equation (1) may be written as

$$u = (T_{eq}/20\ \mathrm{K})^{n+4} . \quad (2)$$

We assume that small grains radiate a total power which is linearly proportional to the energy density, with a spectrum S_ν that is independent of the energy density. For a fixed spectrum of the heating radiation, these assumptions ignore the destruction of the smallest grains at high energy density (Ryter, Puget, and Pérault 1987) and multiphoton processes in the heating of intermediate-size grains (Désert, Boulanger, and Shore 1986). The wavelength at which the emission of a small grain peaks increases with the size of the grain (Désert, Boulanger, and Shore 1986). Therefore, the destruction of the smallest grains primarily reduces the emission at short wavelengths; on the other hand, temperature fluctuations of intermediate-size grains modify the emission at long wavelengths.

We associate the temperature $T_i = h\nu_i/k$ with a frequency ν_i; then the color ratio $I_\nu(\nu_i)/I_\nu(\nu_j)$ can be written as

$$\frac{I_\nu(\nu_i)}{I_\nu(\nu_j)} = \frac{T_i^{n+3}[\exp(T_i/T_{eq}) - 1]^{-1} + CS_\nu(\nu_i)T_{eq}^{n+4}}{T_j^{n+3}[\exp(T_j/T_{eq}) - 1]^{-1} + CS_\nu(\nu_j)T_{eq}^{n+4}} , \quad (3)$$

where C is a normalization constant given by

$$C = \frac{f}{1-f}\frac{k}{h}\frac{\Gamma(n+4)\zeta(n+4)}{\int S_\nu\, d\nu} . \quad (4)$$

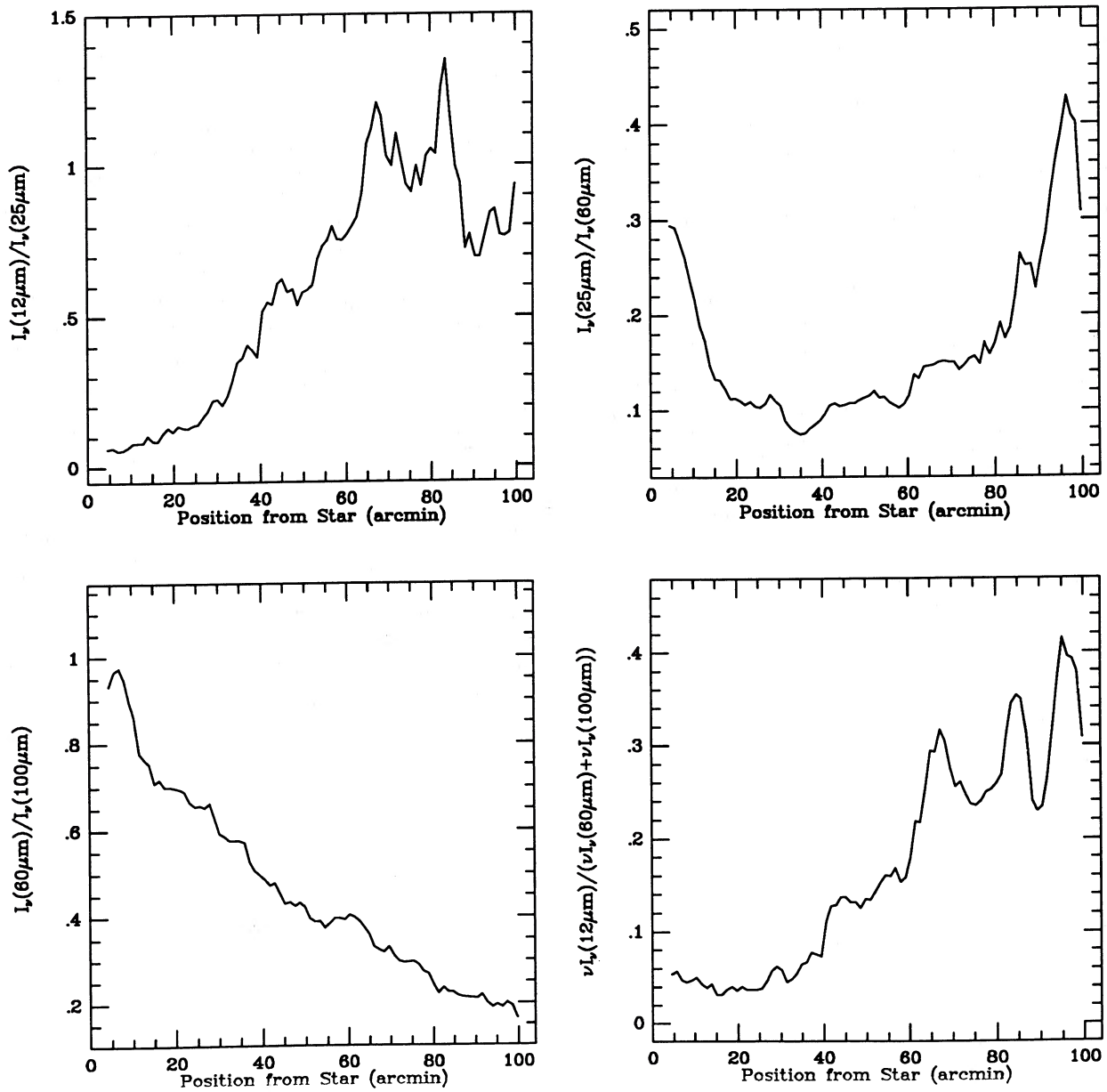

FIG. 3.—Color profiles derived from the emission profiles of Fig. 2

In this last equation f is the fraction of the total emission from dust which comes from small grains, Γ is the gamma function, and ζ is the Riemann zeta function. In this formalism, the relative contribution of small and large grains is a function of the normalization constant C, which depends primarily on the abundance of small grains, and the spectrum S_ν, which is a complicated function of the energy distribution of the heating photons and the size distribution of the small grains.

To compare the model with the data, we need to know the *IRAS* colors of the spectrum S_ν, and the fraction f. Far from the star all of the 12 and 25 μm emission comes from small grains, and the data may be used to estimate the value of the $S_\nu(12\ \mu m)/S_\nu(25\ \mu m)$ color; we find an average value of 0.9. The two other ratios, $S_\nu(25\ \mu m)/S_\nu(60\ \mu m)$ and $S_\nu(60\ \mu m)/S_\nu(100\ \mu m)$, cannot be directly determined from the data because large grains contribute significantly to the 60 and 100 μm emission at all energy densities. In the following we assume that $S_\nu \propto \nu^{0.5}$ at $\lambda > 25\ \mu m$; for this spectrum the ratios $S_\nu(25\ \mu m)/S_\nu(60\ \mu m)$ and $S_\nu(60\ \mu m)/S_\nu(100\ \mu m)$ have values 0.65 and 0.77, respectively.

The fraction f can be estimated from the average spectrum of the infrared emission at Galactic latitude $|b| > 10°$ presented by Boulanger and Pérault (1988). For this spectrum the emission integrated over the 12 μm band of *IRAS* is equal to 10% of the total energy absorbed by dust; combining this number with the colors given in the preceding paragraph, we find that the sum of the four *IRAS* in-band fluxes is equal to 20% of the total emission of dust. To compute the total emission from small grains, we interpolate between the *IRAS* bands and use the observations of Sellgren *et al.* (1985) to estimate the emis-

sion at $\lambda < 7.5$ μm. We find that the emission from small grains represents about 45% of the total energy absorbed by dust, with most of this emission radiated at $\lambda < 35$ μm. This fraction is lower than 45% at high energy densities because some of the small grains get destroyed. For simplicity in the model we ignore the destruction of small grains and use a constant value of 45% for all energy densities.

The results of a model where the emissivity of the large grains was chosen to be proportional to ν are presented in Figure 4. The three colors $I_\nu(12\ \mu m)/I_\nu(25\ \mu m)$, $I_\nu(25\ \mu m)/I_\nu(60\ \mu m)$, and $I_\nu(60\ \mu m)/I_\nu(100\ \mu m)$ follow similar curves shifted in temperature. The $I_\nu(12\ \mu m)/I_\nu(25\ \mu m)$ curve starts with a plateau which covers the range of temperatures where the emission at both frequencies is dominated by small grains; after the plateau there is a drop which is due to an increasing contribution of large grains at 25 μm. In the $I_\nu(25\ \mu m)/I_\nu(60\ \mu m)$ curve the minimum occurs when the large grains start contributing about half of the emission at 25 μm. Measurements in the California Nebula approximately cover the range of equilibrium temperatures 20–50 K. In this range of temperature the model gives color–energy density curves in qualitative agreement with the color profiles of Figure 3.

IV. DISCUSSION

a) *Destruction of Small Grains*

The results of the model are compared with the data in the two color-color diagrams of Figure 5; in each diagram the dotted line was computed from the model by assuming a uniform density of matter around the star and by integrating the emission along the line of sight up to the radius where the star stops being the main source of radiation; these lines show qualitatively how the integration along the line of sight can affect the observed colors. In both diagrams our simple model which ignores the destruction of particles emitting at 12 μm with increasing energy density (§ II) agrees with the data for distances to ξ Per larger than 60′, a distance at which the energy density u is 16 times larger than the ultraviolet energy density of the ISRF, u_{ISRF}. On the other hand, the measured values of $R(12, 60 + 100)$ drop rapidly below the curve of the model for distances smaller than 60′ down to a distance of about 34′ ($u \approx 50u_{ISRF}$), where the data stabilize at a value about 5 times smaller than the prediction of the model; no similar decline is seen for the 25 μm emission.

In the two color-color diagrams the results of the model could be brought into agreement with the data by reducing the 12 μm emission with respect to the emission at the three other wavelengths. The drop in the 12 μm intensity is most probably the result of a destruction of small grains in regions of intense ultraviolet radiation; following this line of interpretation, we find that 80% of the 12 μm emitters present in regions of low energy density are destroyed in regions with $u > 50u_{ISRF}$. The absence of a drop in the 25 μm to far-infrared emission ratio similar to that observed for the 12 μm emission suggests that there is no destruction of the small grains emitting at 25 μm. However, this interpretation is questionable because the temperature fluctuations of intermediate-size grains (which are poorly represented by our two-component model) are critical to the 25 μm emission at high energy densities.

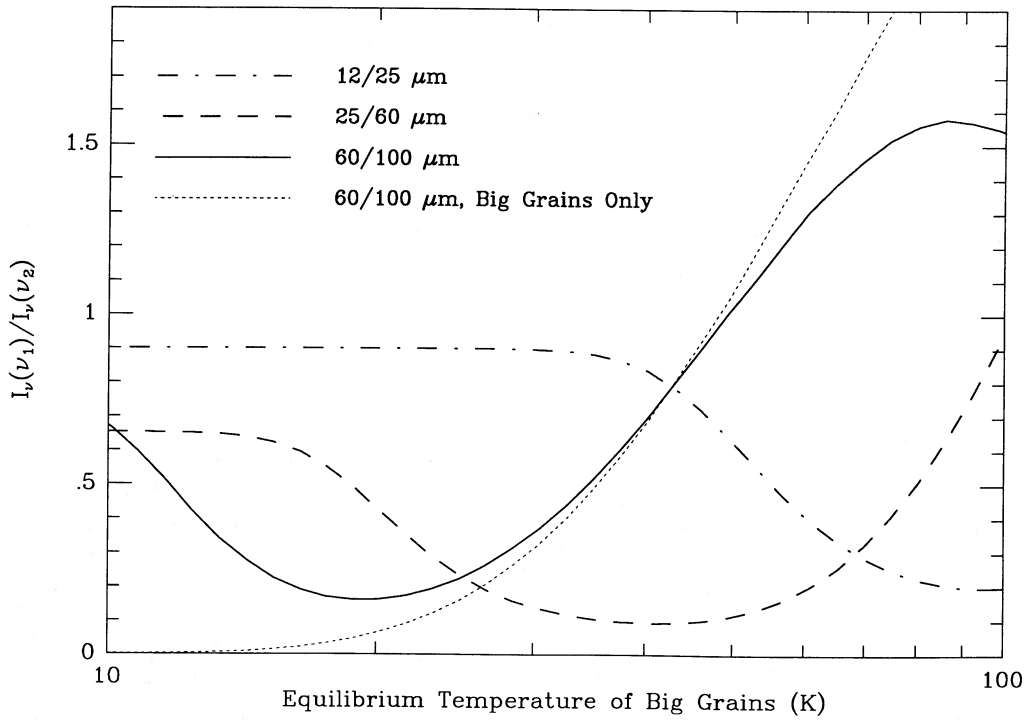

FIG. 4.—$I_\nu(12\ \mu m)/I_\nu(25\ \mu m)$, $I_\nu(25\ \mu m)/I_\nu(60\ \mu m)$, and $I_\nu(60\ \mu m)/I_\nu(100\ \mu m)$ colors computed from the analytical model presented in § III. The emission from small grains represents 45% of the total emission of dust; the emissivity of the large grains is proportional to the frequency. The dotted line gives the $I_\nu(60\ \mu m)/I_\nu(100\ \mu m)$ color for large grains alone.

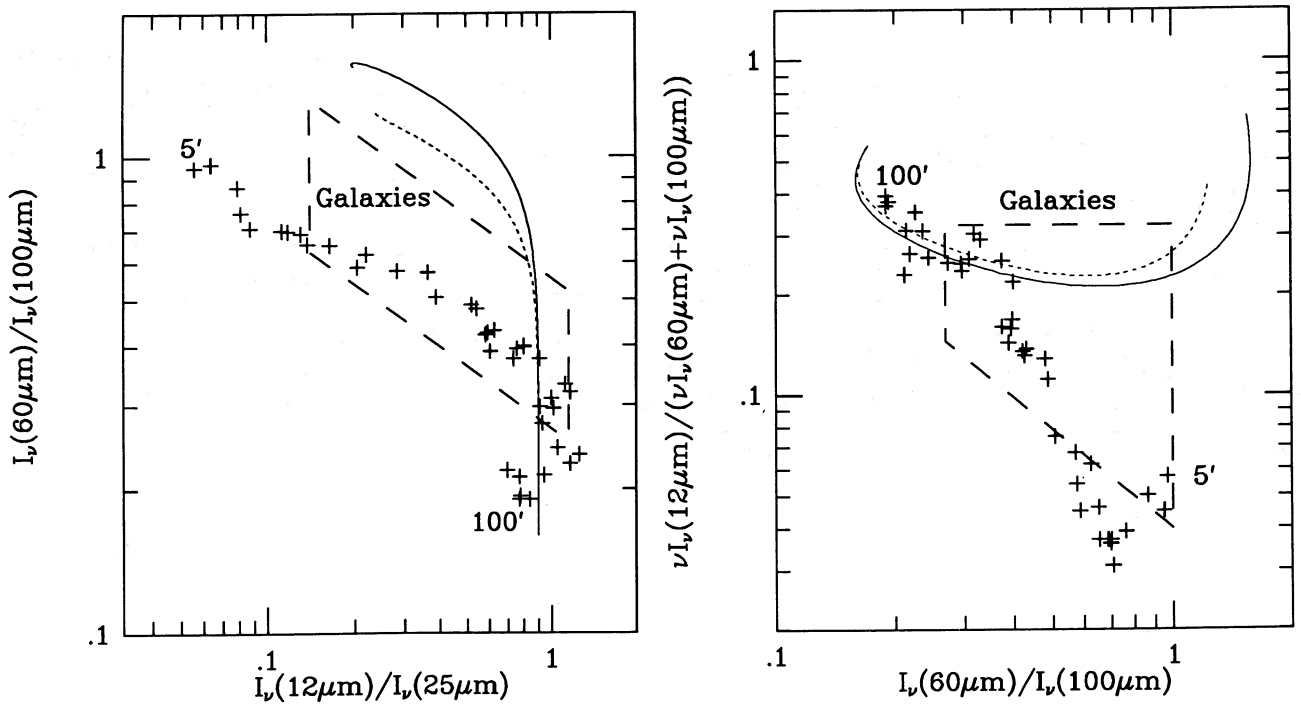

FIG. 5.—*Left:* Distribution of the data points in a $I_\nu(12\ \mu m)/I_\nu(25\ \mu m)$–$I_\nu(60\ \mu m)/I_\nu(100\ \mu m)$ color-color diagram. *Right:* Variation of the 12 μm to far-infrared emission ratio with the $I_\nu(60\ \mu m)/I_\nu(100\ \mu m)$ color. Crosses correspond to color measurements for distances to ξ Per going from 5′ to 100′ at spacings of 2′.3 along the profiles of Fig. 3. The $I_\nu(60\ \mu m)/I_\nu(100\ \mu m)$ color, which is a monotonic function of the distance, may be used to follow the order of the points. The dashed line outlines parts of the diagrams occupied by galaxies (Helou 1986). Full and dotted lines represent the results of the model for equilibrium temperatures ranging from 17 to 100 K; the dotted line was computed from the model by assuming that the density of matter is uniform around the star, and by integrating the emission along the line of sight up to the radius where the star stops to be the main source of radiation.

b) Comparison with Galaxies

The colors measured in the California Nebula follow in the $I_\nu(12\ \mu m)/I_\nu(25\ \mu m)$–$I_\nu(60\ \mu m)/I_\nu(100\ \mu m)$ color-color diagram of Figure 5 a sequence similar to that of galaxies (Helou 1986; Pajot *et al.* 1986). This result shows that the sequence of galaxies from low to high $I_\nu(60\ \mu m)/I_\nu(100\ \mu m)$ ratios and high to low $I_\nu(12\ \mu m)/I_\nu(25\ \mu m)$ ratios corresponds to an increase in the intensity of the radiation field in the regions which are responsible for the infrared emission. For galaxies where starlight is the heating source of dust, the intensity of the radiation field is directly related to the density of young stars; thus, the position of a galaxy along the color-color sequence may be considered as a measure of recent star formation activity (Helou 1986). Figure 4 indicates that the scatter of galaxies perpendicular to the average sequence can result from differences in the content of small grains or, as suggested by Helou (1986), from changes in the fraction of the emission which comes from active regions. The ratio between mid-infrared and far-infrared emission, $\nu I_\nu(12\ \mu m)/[\nu I_\nu(60\ \mu m) + \nu I_\nu(100\ \mu m)]$, which depends primarily on the abundance of small grains, may be used in each individual case to discriminate between these two effects.

V. CONCLUSION

The variation of infrared colors with the energy density has been investigated using *IRAS* observations of the California Nebula. Colors cannot be explained without taking into account emission from small particles which are not in thermal equilibrium with the radiation field; these particles contribute 45% of the infrared emission wherever the energy density in ultraviolet photons, u, is smaller than 16 times the energy density of the ultraviolet part of the average interstellar radiation field, u_{ISRF}. At higher energy densities, the color variations indicate a progressive destruction of the small grains emitting at 12 μm; we estimate that about 80% of these small grains are destroyed in regions where u is larger than $50u_{ISRF}$.

In a color-color diagram $I_\nu(60\ \mu m)/I_\nu(100\ \mu m)$ versus $I_\nu(12\ \mu m)/I_\nu(25\ \mu m)$, colors measured in the California Nebula follow a sequence similar to that of galaxies. This observational result shows that galaxies are distributed along this sequence according to the intensity of the radiation field in the regions responsible for the infrared emission; for normal galaxies where young stars are the dominant heating source of dust the position of galaxies along the sequence is related to recent star formation activity.

REFERENCES

Andriesse, C. D. 1978, *Astr. Ap.*, **66**, 169.
Bohlin, R. C., Savage, B. D., and Drake, J. F. 1978, *Ap. J.*, **224**, 132.
Bohnenstengel, H. D., and Wendker, H. J. 1976, *Astr. Ap.*, **52**, 23.
Boulanger, F., and Pérault, M. 1988, *Ap. J.*, **330**, in press.
Castelaz, M. W., Sellgren, K., and Werner, M. W. 1987, *Ap. J.*, **313**, 853.
Cox, P., Krugel, E., and Mezger, P. G. 1986, *Astr. Ap.*, **155**, 380.
Désert, F. X., Boulanger, F., and Shore, S. 1986, *Astr. Ap.*, **160**, 295.
Draine, B. T., and Anderson, N. 1985, *Ap. J.*, **292**, 494.
Draine, B. T., and Lee, H. M. 1984, *Ap. J.*, **285**, 89.
Elmegreen, D. M., and Elmegreen, B. G. 1978, *Ap. J.*, **219**, 105.
Garmany, C. D., Conti, P. S., and Chiosi, C. 1982, *Ap. J.*, **263**, 777.
Helou, G. 1986, *Ap. J. (Letters)*, **311**, L33.

Hoffleit, D., and Jaschek, C. 1982, *The Bright Star Catalogue* (4th ed.; New Haven: Yale University Observatory).
Léger, A., and Puget, J. L. 1984, *Astr. Ap.*, **137**, L5.
Mathis, J. S., Mezger, P. G., and Panagia, N. 1983, *Astr. Ap.*, **128**, 212.
Morton, D. C. 1969, *Ap. J.*, **158**, 629.
Pajot, F., Boisse, P., Gispert, M., Lamarre, J. M., Puget, J. L., and Serra, G. 1986, *Astr. Ap.*, **157**, 393.
Price, S. 1981, *A.J.*, **86**, 193.
Puget, J. L., Léger, A., and Boulanger, F. 1985, *Astr. Ap.*, **142**, L19.
Ryter, C., Puget, J. L., and Pérault, M. 1987, *Astr. Ap.*, **186**, 312.
Sellgren, K., Allamandola, L. J., Bregman, J. D., Werner, M. W., and Wooden, D. H. 1985, *Ap. J.*, **299**, 416.
Sellgren, K., Werner, M. W., and Dinerstein, H. L. 1983, *Ap. J.* (*Letters*), **271**, L13.
Snow, T. P., and Jenkins, E. B. 1977, *Ap. J. Suppl.*, **33**, 269.
Ungerechts, H., and Thaddeus, P. 1987, *Ap. J. Suppl.*, **63**, 645.
Walborn, N. R. 1972, *A.J.*, **77**, 312.

C. Beichman, F. Boulanger, and G. Helou: Infrared and Processing Analysis Center, Caltech 100-22, Pasadena, CA 91125

F. X. Désert: Laboratory of Astronomy and Solar Physics, Goddard Space Flight Center, Code 685, Greenbelt, MD 20771

M. Péraült: Radio-Astronomie, Ecole Normale Supérieure, 24 rue Lhomond, 75231 Paris Cedex 05, France

C. Ryter: DPh/Ep/Ap, Centre d'Etudes Nucléaires de Saclay, 91191 Gif-sur-Yvette Cedex, France